PROCEEDINGS, 51st Workshop on Geothermal Reservoir Engineering
Stanford University, Stanford, California, February 9-11, 2026
SGP-TR-230

On the Detectability and Appraisal of Hydraulic Fractures Generated with Electrically Conductive Proppant at the Utah FORGE Site Using Borehole Electromagnetic Measurements

Axel Jeconiah, Weichen Zhan, Wardana Saputra, Cristian F. Dominguez, Durra H. Saputera, Carlos Torres-Verdín, Cheng Chen, Parisa Bazazi, and Jennifer Miskimins

Hildebrand Austin Department of Petroleum and Geosystems Engineering, The University of Texas at Austin, Gary L. Thomas Energy Engineering Building (GLT), Room 4.236, 200 E Dean Keeton St, Austin, 78712

axeljeconiah@utexas.edu

Keywords: enhanced geothermal system (egs), triaxial electromagnetic (em) logging, propped fracture imaging, fracture connectivity, reservoir characterization, inversion methods, low-frequency electromagnetics.

ABSTRACT

As enhanced geothermal systems (EGS) continue to gain attention, the ability to engineer and quantify fracture connectivity becomes increasingly important. A critical aspect of this process is understanding proppant placement within fractures, as it directly impacts hydraulic conductivity and guides decisions on (a) where to best intersect fractures for optimal flow paths, or (b) which well completion technique needs to be implemented. Current methods of fracture detection, such as microseismic monitoring or proppant tracers often cannot uniquely resolve proppant distribution far from the borehole, thereby introducing high uncertainty when determining which fracture regions are hydraulically conductive. In this study, we advance the application of triaxial borehole electromagnetic (EM) measurements for detecting and imaging propped fracture geometry in geothermal fields as an alternative/addition to the current fracture detection and appraisal methods to reduce uncertainty. As a preliminary study, we performed numerical simulation of EM measurements in the presence of fractures for both open- and cased-hole completions. Fracture geometries were simulated using ResFrac, providing realistic representations of stimulated areas, and then modeled in COMSOL to evaluate the synthetic triaxial borehole EM response of fractures injected with electrically conductive proppant. Simulation results indicate that borehole instruments with spacings of 100 m, operated at low frequencies (100 Hz), are required to detect the full extent of stimulated fractures. For fracture imaging, a combined strategy is recommended: Long-spacing, low-frequency measurements provide information on the overall extent of proppant-filled fractures, while short-spacing, higher-frequency measurements yield more precise information on fracture locations and type along the borehole. These findings support the development of new inversion methods for imaging the propped fracture geometry, enabling more accurate analysis of fracture connectivity in the field and ultimately improving the ability to ensure robust hydraulic communication between injector and producer wells in EGS.

1. INTRODUCTION

High drilling costs in high-temperature formations and uncertainty in long-term reservoir performance motivate improved methods for describing hydraulically stimulated fractures in enhanced geothermal systems (EGS). In both hydrocarbon and geothermal reservoirs, fracture geometry and proppant placement strongly influence effective flow and stimulated volume and, therefore, recovery and heat-extraction performance. However, commonly used monitoring methods such as microseismic imaging primarily reveal fracture activation rather than proppant distribution, and other diagnostic methods often provide indirect or non-unique estimates of proppant placement (Palisch et al., 2018; Palisch et al., 2016).

Electrically conductive proppants give rise to a conductivity contrast with embedding rocks that can be detected and imaged using electromagnetic (EM) measurements. Prior studies have explored several approaches, including surface EM arrays, borehole resistivity logging, and cross-well methods (Palisch et al., 2018; Palisch et al., 2016; Ahmadian et al., 2018.; Yang et al., 2016; Yang et al., 2013). For deep geothermal settings, borehole EM measurements can reduce surface-to-depth attenuation and improve sensitivity to fracture-scale conductivity anomalies. Recent numerical studies using integral-equation and finite-element solvers have verified that triaxial borehole EM tools can detect conductive fracture targets and, in some cases, support inversion/imaging of simplified fracture geometries (Yang et al., 2016).

This work evaluates the detectability of hydraulically stimulated fractures filled with electrically conductive proppant in a resistive granitic host rock representative of the Utah FORGE site (Jones et al., 2024). We numerically simulate nine-component triaxial induction measurements acquired along the borehole using COMSOL, including the effects of conductive steel casing through a transition boundary condition (TBC). The paper first benchmarks COMSOL results against an independent 2D axisymmetric forward algorithm. We then quantify detection range as a function of tool spacing and frequency, and evaluate sensitivity to realistic fracture conductivity distributions generated from ResFrac outputs. All results in this paper are based on synthetic forward modeling using COMSOL. Future work will incorporate field data for further validation.

2. TECHNICAL BACKGROUND

The simulations in this paper are based on synthetic triaxial borehole electromagnetic (EM) measurements modeled in COMSOL that include nine complex voltage components, V_{ij}. These tensor measurements provide directional sensitivity that can help to constrain fracture orientation and geometry. For conditions involving conductive steel casing, we model casing effects using a transition boundary condition (TBC) to avoid meshing the thin casing wall explicitly. This section also describes the selection of formation and proppant electrical conductivities used in the study.

2.1 Triaxial Tool

EM induction tools enforce an alternating current (AC) through a coil to generate a primary magnetic field. This primary field induces eddy currents in the formation and within any conductive fracture fill, which in turn generate a secondary field measured by receiver coils as complex-valued voltages. A triaxial tool uses three orthogonal transmitter coils and three orthogonal receiver coils, yielding a nine-component complex measurement set, V_{ij}, with real and imaginary parts, where V_{ij} is defined as the measured voltage of the receiver coil, i denotes the receiver orientation, while j denotes the transmitter orientation. These components provide sensitivity to dominant fracture direction and spatial asymmetry. Multiple receivers can be used to increase depth of investigation and improve the information content for inversion/imaging. Figure 1 describes the triaxial configuration and tool orientation in the borehole assumed in our study.

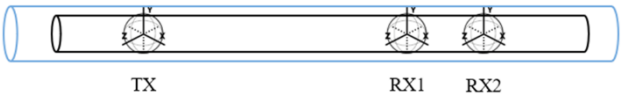

Figure 1: Triaxial tool configuration inside a borehole. The transmitter (TX) is on the left and the two receivers (RX1 and RX2) are on the right side. TX-RX spacings and frequencies are tuned for the specific application and expected fracture conditions.

When deployed in the field, the tool assembly will move together along the borehole, and the transmitter coils will be energized one at a time. The usage of signal amplifiers and bucking coils is common practice in borehole acquisition of EM measurements.

2.2 Transition Boundary Condition (TBC)

Steel casing strongly modifies borehole EM measurements due to its high electrical conductivity and small wall thickness (Heagy, 2018). Explicitly meshing the casing volume can require extremely fine elements across the wall thickness, which increases degrees of freedom, memory requirements, and computational cost. To reduce meshing requirements while accurately retaining EM casing effects, we model the casing using a transition boundary condition (TBC), which represents a thin conductive layer through an effective boundary formulation.

The accuracy of the TBC approximation depends on operating frequency, casing thickness, and electrical conductivity contrast. We validate the use of TBC in our workflow by comparing COMSOL calculations against an independent 2D axisymmetric EM forward algorithm under cased-hole conditions, assuming a straight borehole, axially homogeneous properties, and a homogeneous background formation.

2.3 Proppant and Formation Conductivity

EGS are commonly implemented in crystalline basement rocks that have elevated temperatures, motivating the use of a resistive granitic formation as part of the model. Granite resistivity is typically higher than that of sedimentary rocks, which increases the conductivity contrast relative to electrically conductive proppant, hence improving EM detectability (Pardo and Torres-Verdín, 2013).

Several electrically conductive proppant options have been proposed in the past, including metallic proppants and advanced coated materials, but these can be costly and may require blending strategies that introduce uncertainty in bulk conductivity (Palisch et al., 2018; Palisch et al., 2016; Zhang et al., 2021). We therefore consider petroleum coke (PC) as a candidate for electrically conductive proppant because it is commercially available and can provide elevated bulk conductivity relative to typical proppant materials. Material-property assumptions used in this study are summarized in Table 1. The formation electrical conductivity is representative of the Utah FORGE site.

3. MODEL

This section summarizes the model geometries for the conditions investigated in the study. Electrical and geometric properties are tabulated for ease of reference. We also describe the procedure used to obtain the conductivity model for a realistic fracture geometry.

3.1 Validation Model

COMSOL results were benchmarked against an independent 2D axisymmetric EM forward modeling code (AHM) (Wang et al., 2009). For both open- and cased-hole completions were analyzed. Because the benchmark models are 2D axisymmetric, the comparison is restricted to disk-shaped fractures centered along the tool axis, and only the ZZ component of the triaxial measurement tensor is evaluated. For the validation conditions, the fracture radius, R, was set to match the transmitter–receiver spacing of the benchmark cases (2.54 m and 38.837 m). Here, “fracture radius” refers to the disk radius geometry, R, shown in Figure 2.

In this study, the borehole axis is aligned with the *z*-direction, and the tool is translated along the *z*-axis during logging. An open-hole completion is described in Figure 2 (left), while the cased-hole completion is illustrated in Figure 2 (right). The black dashed line indicates the tool path, as well as the model axis of symmetry. The fracture is indicated in red, and its radius, *R*, varies depending on the condition. Table 1 summarizes the electrical and geometric parameters used for each validation case.

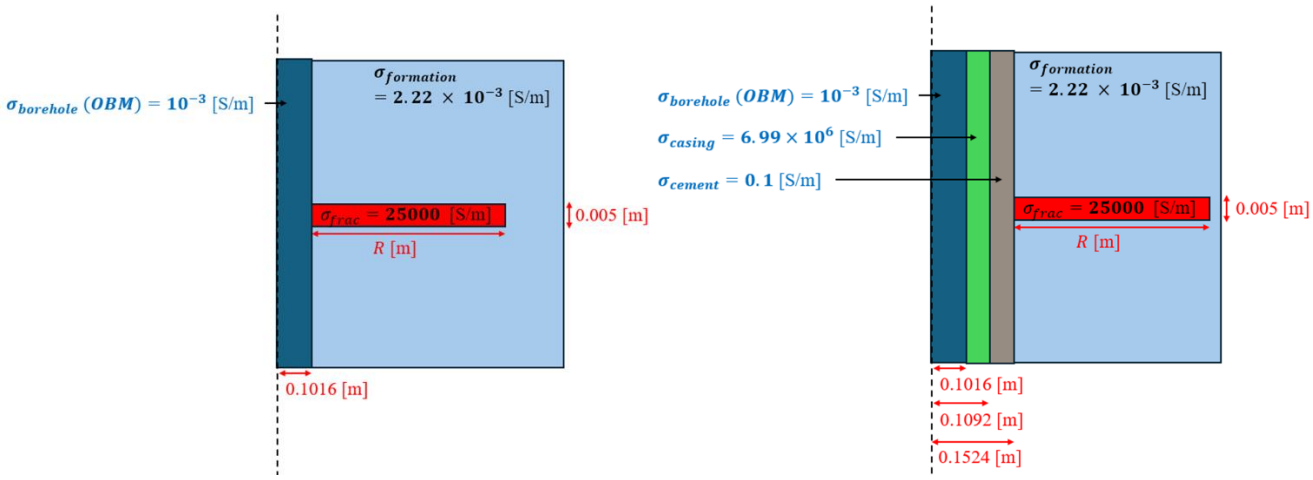

Figure 2: Validation model geometries used for benchmarking. Left: open-hole completion. Right: cased-hole completion modeled using a transition boundary condition (TBC). The fracture is represented as a conductive disk of radius *R* (red). The black dashed line indicates the logging path of the triaxial tool. Electrical properties assumed for the formation, borehole fluid, casing, and cement are highlighted.

Table 1: Electrical and geometric parameters used for each validation condition.

Features	Condition 1: Open-Hole Validation, Short Spacing	Condition 1.1: Open-Hole Validation, Long Spacing	Condition 2: Cased-Hole Validation, Short Spacing	Condition 2.1: Cased-Hole Validation, Long Spacing
Operating Frequency	100 Hz	100 Hz	100 Hz	10 Hz
Fracture Radius, *R*	2.54 m	38.837 m	2.54 m	38.837 m
Tool Spacing	2.54 m	38.837 m	2.54 m	38.837 m

A casing thickness of 0.76 cm was assumed for all conditions. Casing and cement conductivities are 6.99 x 10^6 S/m and 0.1 S/m, respectively. The borehole fluid is modeled as oil-based mud with a conductivity of 10^{-3} S/m. Measured depth (MD) is defined such that MD = 0 m corresponds to the fracture centered midway between the transmitter and receiver. Unless otherwise stated, the fracture thickness is 5 mm. Condition 2.1 assumes a 10 Hz operating frequency because the 2D benchmark forward model produced inconsistent results at 100 Hz for the cased-hole long-spacing configuration.

3.2 Model for Fracture Radius Sensitivity Analysis (SA)

The model constructed for fracture length sensitivity analysis is based on the validation geometry shown in Figure 2 (right). Three transmitter–receiver spacings (13.208 m, 38.837 m, and 100 m) were chosen to cover the investigated range of fracture radius. For each spacing, the fracture is centered midway between the transmitter and receiver, and the fracture radius progressively increases to represent increasing fracture extent away from the borehole. Operating frequencies of 10 Hz, 100 Hz, 1 kHz, and 10 kHz are evaluated for each spacing.

3.3 Complex Fracture Network (CFN) Model

A key uncertainty in hydraulic fracturing is whether the stimulated fracture volume can be represented as a single planar feature or a complex fracture network (CFN) with multiple interacting branches. To investigate the effect of geometric complexity on EM detectability, we construct a synthetic complex fracture network (CFN) model based on the multiple planar fractures shown in Figure 3. The CFN consists of five 1 mm-thick fractures separated by 0.2 m, where the leading fracture is positioned right after the cement, and the remaining fractures are staggered behind it by 0.5 m to mimic a branched network that could form during stimulation. In this work, we

emphasize planar fracture cases because granitic EGS targets at depth often exhibit dominantly planar propagation controlled by the minimum principal stress; however, the CFN model provides an initial test of sensitivity to non-planar complexity.

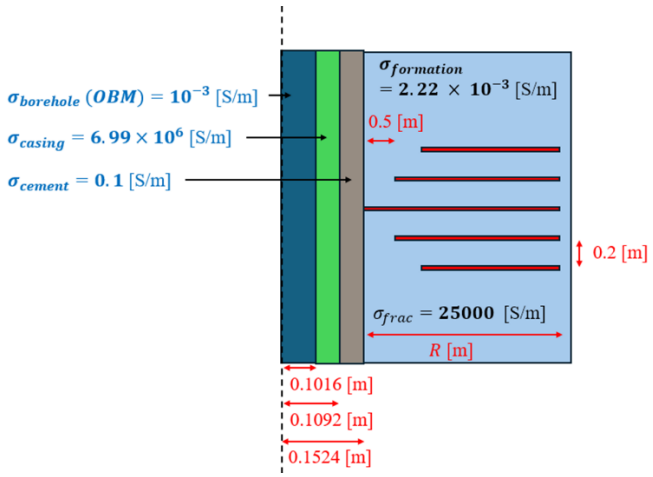

Figure 3: Complex fracture network (CFN) model consisting of five 1 mm-thick fractures. The fracture radius is R = 38.837 m, the spacing between consecutive fractures is 0.2 m, and the fractures are staggered by 0.5 m behind the leading fracture to represent branching. All other electrical properties and well geometry are the same as in the cased-hole validation model.

This model is then used as input to the COMSOL simulations. Two transmitter–receiver spacings are considered for comparison: 1 m and 38.837 m.

3.4 ResFrac Model

A realistic fracture conductivity distribution was generated using ResFrac simulations and then imported into COMSOL as a spatially varying conductivity model. The ResFrac simulation was designed to represent an EGS-like hydraulic stimulation condition in a resistive granitic formation, consistent with conditions relevant to the Utah FORGE site. By changing the formation fracture gradient, two fracture realizations were generated, and the corresponding EM responses were simulated using COMSOL.

From the ResFrac outputs, we extracted the fracture element coordinates and total proppant volume fraction. Total proppant volume fraction was then converted to an effective electrical conductivity using a correlation proposed by Heagy (2018). Because the correlation is fitted primarily for volume fractions above 0.33, and the conductivity variation is low for volume fractions below 0.33, these values were assigned a constant conductivity equal to 100 S/m.

Figure 4 describes the volume-fraction-to-conductivity correlation used in this work. Figure 5 shows the spatial mapping from the ResFrac proppant volume fraction field to the resulting electrical conductivity distribution used in COMSOL.

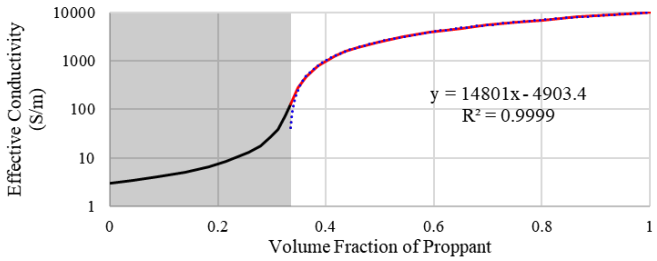

Figure 4: Relationship used to convert total proppant volume fraction from ResFrac into effective fracture electrical conductivity, based on Heagy (2018). A constant conductivity of 100 S/m was assigned for volume fractions below 0.33 (the area shaded in gray).

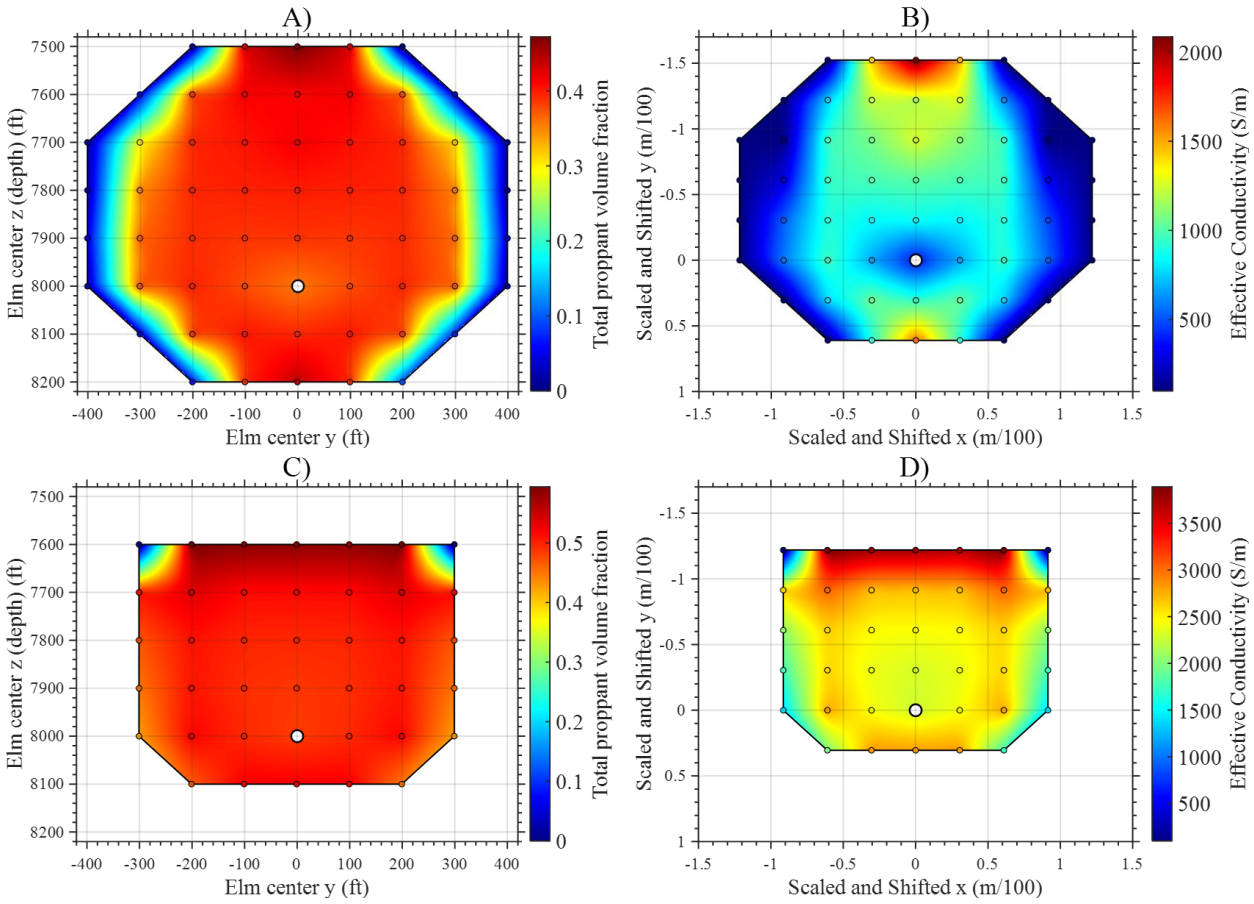

Figure 5: Spatial mapping from ResFrac proppant volume fraction to the electrical conductivity model used in COMSOL. Panels (A) and (C) show the total proppant volume fraction on the fracture plane in the ResFrac coordinate system, where the well is horizontal and the borehole location (white circle) lies along the *x*-axis. Panels (B) and (D) show the corresponding effective conductivity distribution after applying the volume-fraction-to-conductivity conversion and transforming the geometry into the COMSOL coordinate system, where the borehole is represented as a vertical well aligned with the *z*-axis. The model is recentered and scaled as indicated by the axes.

ResFrac provides additional fracture attributes beyond proppant volume fraction, such as fracture aperture, which could also influence effective electrical conductivity. Incorporating aperture into the COMSOL model is not straightforward. One option is to explicitly model fracture thickness within the COMSOL geometry, but this can increase meshing requirements and computational cost. Another option is to convert aperture into an effective conductivity using a conductance-based relationship (e.g., aperture multiplied by conductivity). Because this procedure introduces additional modeling uncertainty and requires further validation, aperture effects are not included in our study.

All remaining model parameters (formation, borehole, casing, and cement) are consistent with the cased-hole validation case. The tool configuration used for the scaled ResFrac-based model is a spacing of 2.54 m operated at 100 Hz.

4. RESULTS

Results confirm the feasibility of using borehole triaxial EM measurements to detect conductive, proppant-filled fracture geometries embedded in a resistive granitic formation. Benchmarking against an independent 2D axisymmetric EM forward algorithm reveals consistent response trends, supporting the use of COMSOL for synthetic EM simulations across different completion conditions and fracture configurations. Sensitivity analyses further indicate that variations in fracture geometry produce percent difference of ~100% in the ZY and YZ tensor components of the simulated responses, motivating future work on inversion/imaging of fracture parameters using multi-component V_{ij} measurements.

4.1 Validation Result

COMSOL results were benchmarked against an independent 2D axisymmetric EM forward algorithm (AHM), yielding strong agreement in response shape for both open- and cased-hole conditions. The percent difference between the two results was computed at each logging point (percent difference between the COMSOL response and the 2D axisymmetric benchmark response). Across the validation cases, the maximum pointwise percent difference was below 1%.

Absolute voltage amplitudes can vary between forward models due to differences in tool source's implementation, normalization, and reference definitions. Accordingly, we focus the comparison on response shape and relative trends rather than raw amplitude. To enable consistent trend comparison, an affine normalization was applied to align both the baseline and dynamic range of each response. The transformation used is given by

$$y_A^{match} = c_B + \frac{\max(y_B) - c_B}{\max(y_A) - c_A}\,(y_A - c_A), \tag{1}$$

where simulation A is scaled to match simulation B. Here, y_A, is the response from simulation A while, y_B, is the response from simulation B. The constants, c_A, and, c_B, represent baseline values (far-field value) for each simulation. This transformation shifts and scales simulation A so that its baseline and maximum amplitude match those of simulation B. Figures 6 and 7 summarize the benchmarking results for the open- and cased-hole conditions, respectively, for both short- and long-spacing tool configurations.

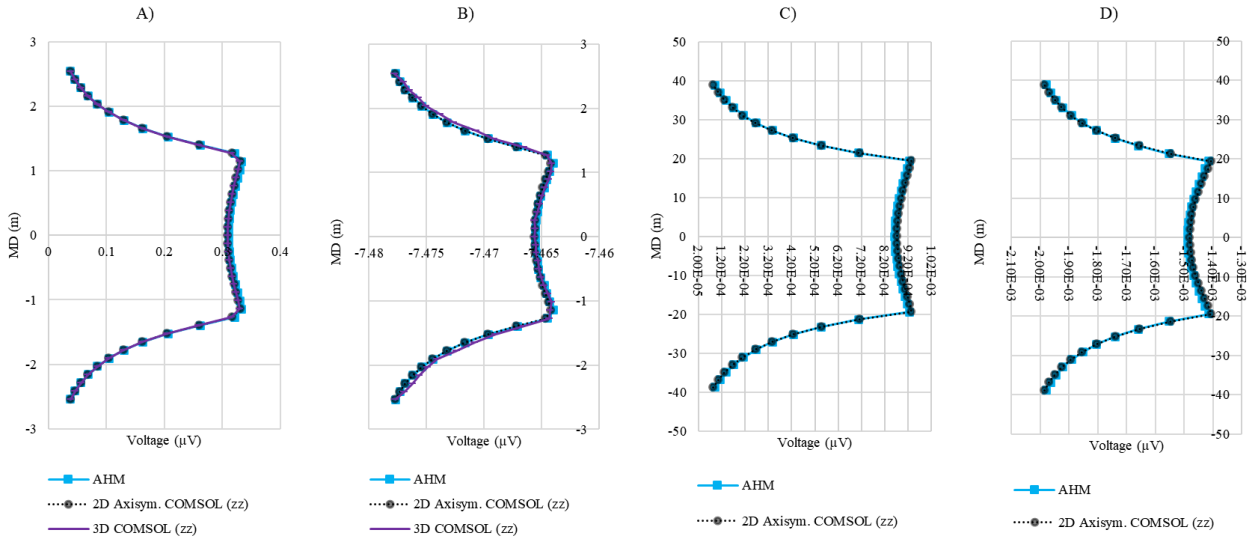

Figure 6: Benchmarking results obtained for the open-hole completion condition (Condition 1 and 1.1). Panels (A–B) describe the short-spacing configuration (2.54 m) at 100 Hz, while panels (C–D) describe the long-spacing configuration (38.837 m) at 100 Hz. Responses are compared between COMSOL and a 2D axisymmetric forward algorithm (AHM) using the V_{zz} real and imaginary components. Panels (A) and (C) are the real V_{zz} component, while panels (B) and (D) are the imaginary V_{zz} component.

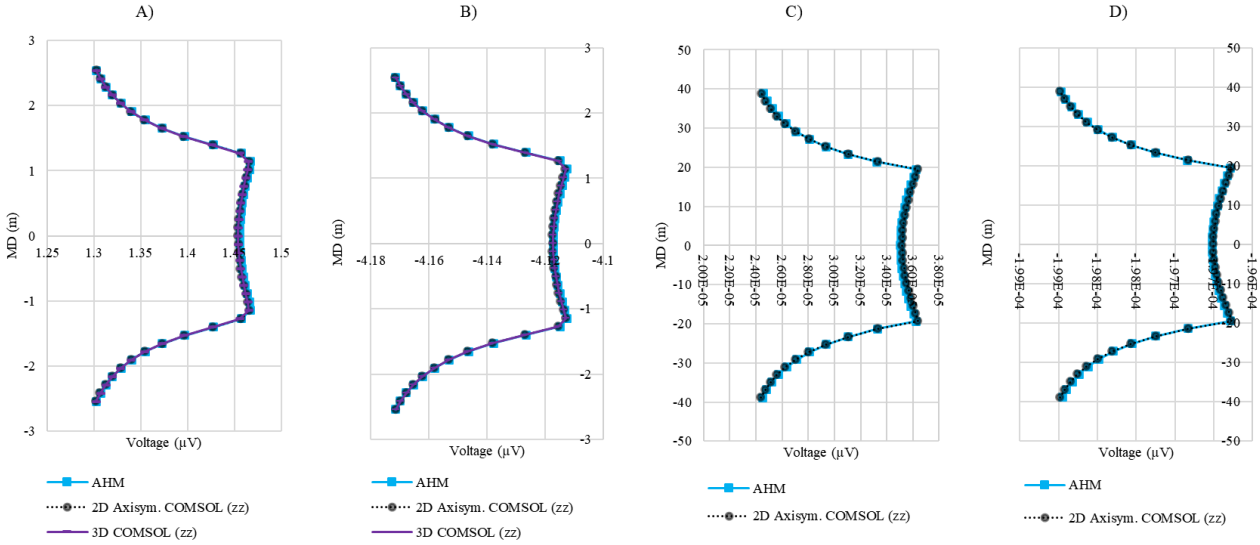

Figure 7: Benchmarking results obtained for the cased-hole completion condition (Condition 2 and 2.1). Panels (A–B) describe the short-spacing configuration (2.54 m) at 100 Hz, while panels (C–D) describe the long-spacing configuration (38.837 m) at 10 Hz. Responses are compared between COMSOL and a 2D axisymmetric forward algorithm (AHM) using the V_{zz}

real and imaginary components. Panels (A) and (C) are the real V_{zz} component, while panels (B) and (D) are the imaginary V_{zz} component.

For the remainder of this paper, all sensitivity analyses are performed under cased-hole conditions. This choice reflects typical completion designs for EGS injection wells and provides a conservative assessment because the conductive casing reduces signal sensitivity to formation features compared to open-hole conditions.

4.2 Fracture Radius Sensitivity Analysis (SA)

A key requirement for triaxial EM fracture appraisal is the ability to detect conductive, proppant-filled fractures at increasing distances from the borehole. To quantify depth of investigation, we evaluate response sensitivity as a function of successive radii for three transmitter–receiver spacings (13.208 m, 38.837 m, and 100 m) over a range of operating frequencies (10 Hz–10 kHz). For each spacing, the fracture is centered midway between the transmitter and receiver, while the fracture radius is increased progressively to represent increasing fracture extent away from the wellbore.

Sensitivity in this section is reported using the pointwise percent difference between responses at successive radii, i.e.,

$$\Delta(R_n) = 100\% \cdot \frac{|V(R_n) - V(R_{n-1})|}{\frac{|V(R_n)| + |V(R_{n-1})|}{2}}, \tag{2}$$

where V is the simulated voltage component (real part of V_{zz}) and $R_n - R_{n-1}$ is the radius step size. Here, the radius increments are 1 m, 5 m, and 10 m for spacings of 13.208 m, 38.837 m, and 100 m, respectively. Figure 8 summarizes the sensitivity trends for all spacings and frequencies considered.

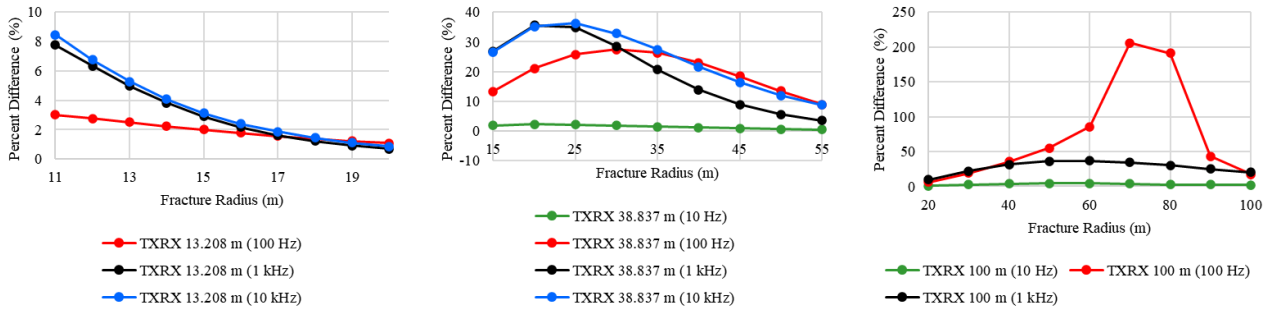

Figure 8: Fracture radius sensitivity analysis for three transmitter–receiver spacings (13.208 m, 38.837 m, and 100 m). Sensitivity is quantified using the pointwise percent difference between simulated responses at successive fracture radii for multiple operating frequencies. All results correspond to the real part of the V_{zz} component with the fracture centered midway between the transmitter and receiver.

For the 13.208 m spacing case, the 10 kHz response exhibits the highest sensitivity, with percent differences remaining on the order of ~5% at R = 13 m. For the 38.837 m spacing case, the 100 Hz response produces the strongest sensitivity, exceeding ~20% near R = 40 m. For the 100 m spacing case, the 100 Hz response exhibits a pronounced sensitivity peak exceeding 200%, which occurs when the response changes sign between successive radii, that decreases down to ~40% near R = 90 m. These trends indicate that the optimal operating frequency depends strongly on tool spacing and target distance, motivating multi-frequency acquisition for robust detectability assessment.

Only the real component of V_{zz} is reported here; the imaginary component exhibits similar trends but with different sensitivity magnitudes depending on frequency. In practice, detectability depends on measurement noise and modeling uncertainty too. Therefore, sensitivity thresholds (e.g., 1–5%) should be interpreted relative to the expected tool noise floor as well as systematic modeling errors.

4.3 Complex vs. Planar Fracture Detection

The CFN results indicate that distinguishing fracture-network complexity from a single planar fracture using borehole EM responses can be challenging, particularly at longer transmitter–receiver spacing. Figure 9 compares the CFN model response (five 1 mm-thick fractures) against a planar fracture model (single 5 mm-thick fracture) for two spacings at 100 Hz. For the long spacing case (38.837 m), both the real and imaginary components exhibit very similar trends for both the CFN and planar models, with minimal observable differences in response shape.

In contrast, the short spacing case (1 m) exhibits clearer shape differences between the CFN and planar responses in both the real and imaginary components. The corresponding pointwise absolute percent difference across logging points remains below ~2%, indicating that the distinction is primarily reflected in subtle changes in response shape rather than amplitude. These results suggest that shorter transmitter–receiver spacing improves sensitivity to near-borehole geometric details, whereas longer spacing primarily reflects the broader-scale fracture response and may be less sensitive to small-scale network complexity.

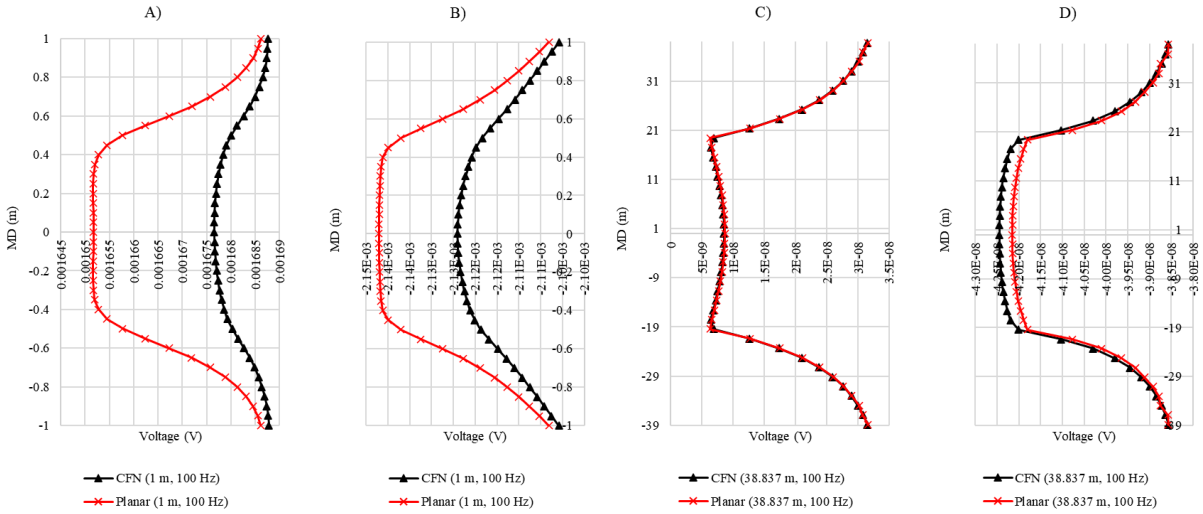

Figure 9: Comparison of simulated responses for a complex fracture network (CFN; five 1 mm-thick fractures) and an equivalent planar fracture (single 5 mm-thick fracture) at 100 Hz. Panels (A–B) show the real and imaginary components for the 1 m transmitter–receiver spacing, while panels (C–D) show the real and imaginary components for the 38.837 m spacing. The 1 m spacing exhibits small but visible shape differences between the CFN and planar responses, whereas the 38.837 m spacing shows nearly identical responses.

Finally, whether these small shape differences can be exploited for robust interpretation will depend on measurement noise and modeling uncertainty. This will be assessed in future work through inversion-based analysis and sensitivity studies.

4.4 Realistic Fracture Geometry Triaxial Sensitivity

Our analysis compares two realistic fracture geometries generated from ResFrac and mapped into COMSOL using the workflow described in Section 3.4. The two cases differ primarily in the formation fracture gradient used in ResFrac, which produces different proppant distributions and resulting fracture asymmetry in the vertical direction. The “low fracture gradient” case yields a larger, more vertically distributed proppant footprint, whereas the “high fracture gradient” case produces a smaller but more asymmetric and concentrated proppant distribution.

Figures 10 and 11 describe the real and imaginary parts of the full nine-component response V_{ij} for a 2.54 m transmitter–receiver spacing at 100 Hz. As expected, cross-components that are not directly excited by the fracture asymmetry (e.g., XY, XZ, YX, and ZX) remain close to zero for both cases. Differences between the two fracture geometries are most evident in components sensitive to asymmetry in the y-direction, particularly ZY and YZ, where the high-gradient case produces larger shape and amplitude changes with pointwise absolute percent difference ~100%. In contrast, co-planar and co-axial components (XX, YY, and ZZ) exhibit smaller relative differences of less than 5% but having noticeable shape differences. These components also have substantially larger response magnitudes—approximately three orders of magnitude higher than the cross-components—making them more robust to measurement noise.

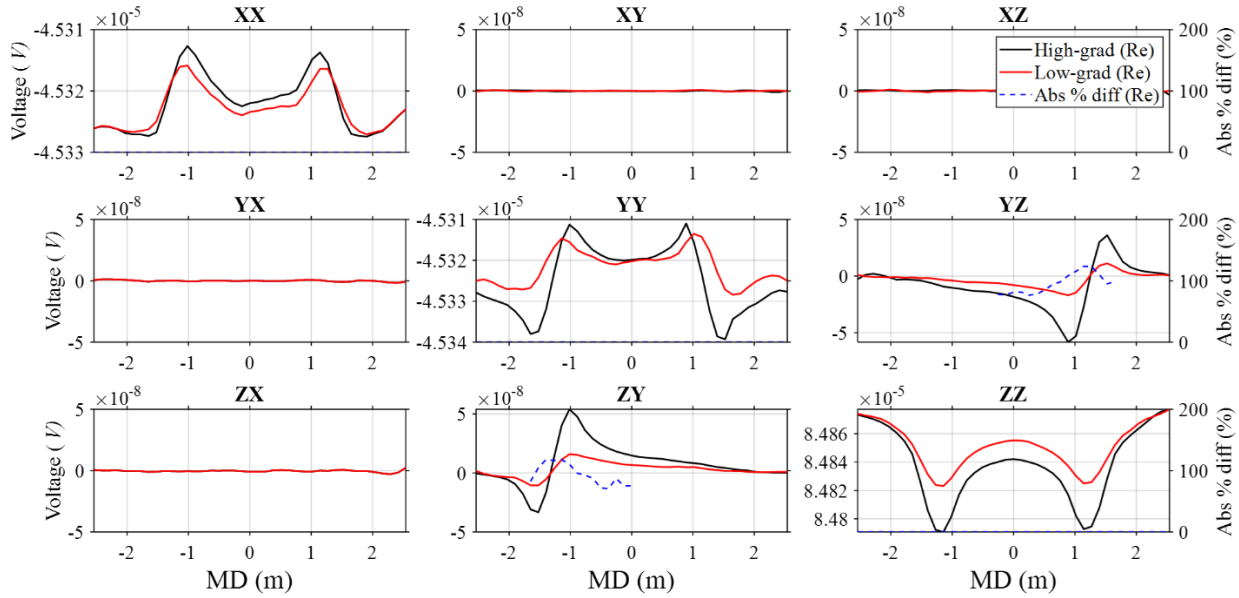

Figure 10: Real part of simulated V_{ij} for two ResFrac-derived fracture conductivity models ("low fracture gradient" and "high fracture gradient") simulated in COMSOL using a 2.54 m transmitter–receiver spacing at 100 Hz. The plotted curves are smoothed using a 7-point Savitzky–Golay filter for visualization. The dashed curve shows the pointwise absolute percent difference between the two cases for selected components.

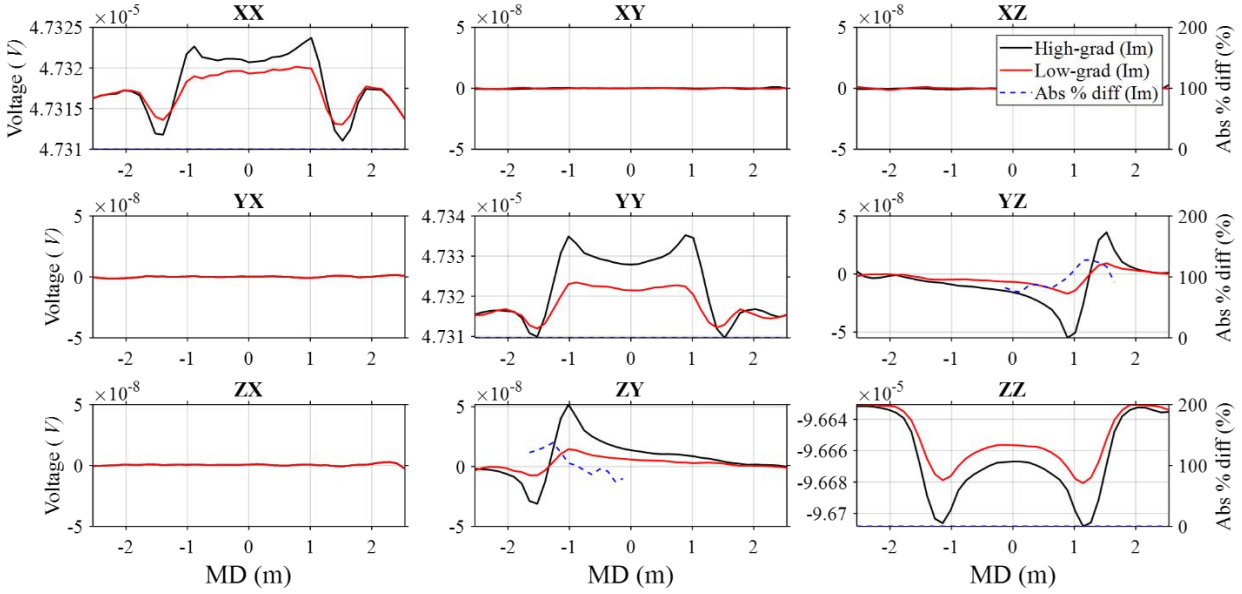

Figure 11: Imaginary part of simulated V_{ij} for the same two ResFrac-derived fracture conductivity models, simulated using a 2.54 m transmitter–receiver spacing at 100 Hz. The plotted curves are smoothed using a 7-point Savitzky–Golay filter for visualization. Differences are most apparent in off-diagonal components sensitive to fracture asymmetry.

Overall, these results indicate that multi-component EM triaxial measurements can capture subtle geometric differences between realistic proppant distributions, with the greatest sensitivity appearing in off-diagonal components and associated with fracture asymmetry. The magnitude of these differences should be interpreted relative to expected noise levels in field measurements; increasing the number of receivers and using multiple operating frequencies is expected to improve robustness in future inversion/imaging studies.

5. DISCUSSION

The benchmarking described in this paper is limited to the V_{zz} component because the reference forward algorithms are 2D axisymmetric. Extending the validation to additional tensor components will require full 3D benchmarking and additional independent modeling tools. In addition, all results in this study are synthetic and assume an idealized tool response in a homogeneous background formation.

The realistic fracture conductivity distributions derived from ResFrac also depend on the underlying hydraulic fracturing simulation assumptions. In particular, the modeled fractures primarily propagate as a planar feature controlled by the minimum stress direction. The sensitivity results presented here suggest that the CFN case produces only subtle differences in EM response relative to a planar case for the configurations tested; however, the detectability of stronger geometric complexity (e.g., sharp turns or intersection with natural fault) remains an open question and should be evaluated in future work.

For field deployment, several factors may reduce sensitivity and increase measurement uncertainty. Tool decentralization within the borehole, borehole deviation, and imperfect coil orthogonality can introduce systematic errors, particularly for longer transmitter–receiver spacings. Temperature-dependent effects on electronics and tool calibration may also be significant in high-temperature geothermal environments. Practical detectability depends on tool noise floor and environmental noise; therefore, sensitivity thresholds reported here should be interpreted relative to expected measurement uncertainty, which may vary with frequency, spacing, and temperature conditions.

Results indicate a strong tradeoff between operating frequency and transmitter–receiver spacing. Low frequencies generally increase depth of investigation but may reduce sensitivity to smaller-scale conductivity variations, while high frequencies can enhance near-field sensitivity but experience greater conductive losses. These tradeoffs will be further evaluated in future work using inversion-based analyses.

The 3D simulations also highlight practical computational challenges when modeling fractures in the presence of electrically conductive casing. Smoothing was required to reduce numerical noise associated with meshing limitations, and further mesh refinement would increase computational cost. The 3D simulation results presented in Section 4.4 required approximately 132 hours on a 6-core CPU with 128 GB RAM.

Despite the above limitations, results suggest that triaxial borehole EM measurements have the potential to provide additional constraints on conductive, proppant-filled fracture geometries beyond what is available from standard commercial induction tools, particularly in resistive crystalline formations.

Future work will evaluate the full nine-component response V_{ij}, including the imaginary components, which may provide additional sensitivity to fracture conductivity and geometry depending on frequency and spacing. Incorporating realistic noise and developing inversion/imaging workflows will be key next steps.

6. CONCLUSION

COMSOL benchmarking performed against independent 2D axisymmetric forward algorithms shows strong agreement for the V_{zz} component under both open- and cased-hole conditions, with a maximum pointwise percent error below 1%. Under cased-hole conditions, the real part of V_{zz} indicates sensitivity to conductive fractures out to approximately 90 m, with a ~40% response difference for a fracture radius of $R = 80$ m using a 100 m transmitter–receiver spacing at 100 Hz. Shorter transmitter–receiver spacing increases sensitivity to fracture features closer to the borehole; for example, the 13.208 m spacing at 10 kHz yields a ~5% response difference when the fracture radius increases from 12 m to 13 m.

Comparisons between a complex fracture network (CFN) model and an equivalent planar fracture model indicate that the 1 m spacing produces small but observable response-shape differences, albeit the pointwise absolute percent difference remains below ~2% for the cases tested. Finally, full nine-component triaxial responses indicate sensitivity to geometric asymmetry in realistic ResFrac-derived fracture conductivity models, with the YZ and ZY cross-components exhibiting pointwise absolute percent differences on the order of ~100% between the low- and high-gradient cases. These results support the use of multi-component borehole EM triaxial measurements, combined with multi-spacing and multi-frequency acquisition, to improve constraints on conductive fracture geometry across resistive crystalline formations.

7. ACKNOWLEDGMENT

This work was conducted in collaboration with the Department of Civil, Environmental and Ocean Engineering at Stevens Institute of Technology and the Department of Petroleum Engineering at Colorado School of Mines, and was supported by the U.S. Department of Energy (DOE) under award number # DE-EE0007080 project entitled “Enhanced Geothermal System Concept Testing and Development at the Milford City, Utah Forge Site and by The University of Texas at Austin Research Consortium on Formation Evaluation, which is jointly sponsored by AkerBP, Baker Hughes, bp, Chevron, CNOOC International, ConocoPhillips, Eni, Equinor, ExxonMobil, Fieldwood Energy E&P Mexico, Harbour Energy Norge AS, Halliburton, Oxy, Petrobras, Repsol, SLB, TotalEnergies, and Woodside.

REFERENCES

Ahmadian, M., LaBrecque, D., Liu, Q.H., Slack, W., Brigham, R., Fang, Y., Banks, K., Hu, Y., Wang, D., and Zhang, R.: Demonstration of Proof of Concept of Electromagnetic Geophysical Methods for High Resolution Illumination of Induced Fracture Networks, Proceedings, SPE Hydraulic Fracturing Technology Conference and Exhibition (2018). OnePetro.

Heagy, L.: Electromagnetic Methods for Imaging Subsurface Injections, PhD Dissertation, University of British Columbia (2018).

Jones, C., Simmons, S., and Moore, J.: Geology of the Utah Frontier Observatory for Research in Geothermal Energy (FORGE), Enhanced Geothermal Systems (EGS) Site, Geothermics, 122, (2024), 103054.

Palisch, T., Al-Tailji, W., Bartel, L., Cannan, C., Czapski, M., and Lynch, K.: Recent Advancements in Far-Field Proppant Detection, Proceedings, SPE Hydraulic Fracturing Technology Conference and Exhibition (2016). OnePetro.

Palisch, T., Al-Tailji, W., Bartel, L., Cannan, C., Zhang, J., Czapski, M., and Lynch, K.: Far-Field Proppant Detection Using Electromagnetic Methods: Latest Field Results, SPE Production & Operations, 33(03), (2018), 557–568.

Pardo, D., and Torres-Verdín, C.: *Sensitivity analysis for the appraisal of hydrofractures in horizontal wells with borehole resistivity measurements*, Geophysics, 78(4), (2013), D209–D222, doi:10.1190/GEO2013-0014.1.

Wang, G.L., Torres-Verdín, C., and Gianzero, S.: Fast Simulation of Triaxial Borehole Induction Measurements Acquired in Axially Symmetrical and Transversely Isotropic Media, Geophysics, 74(6), (2009), E233–E249.

Yang, K., Celik, E., Torres-Verdín, C., and Yilmaz, A.E.: Detection and Quantification of 3D Hydraulic Fractures with Multi-Component Low-Frequency Borehole Resistivity Measurements, SEG Technical Program Expanded Abstracts (2013), 545–550.

Yang, K., Yilmaz, A., and Torres-Verdín, C.: Efficient 3D Parametric Inversion of Hydraulic Fractures with Low-Frequency Borehole Triaxial Electromagnetic Measurements, SEG Technical Program Expanded Abstracts (2016), 954–958.

Zhang, P., Ozowe, W., Russell, R.T., and Sharma, M.M.: Characterization of an Electrically Conductive Proppant for Fracture Diagnostics, Geophysics, 86(1), (2021), E13–E20.